Leading edge vortex dynamics

17th Australasian Wind Engineering Society Workshop
Wellington, New Zealand
12-13 February 2015

Leading Edge Vortex Dynamics

P.J. Richards[1] and I.M. Viola[2]

[1]Department of Mechanical Engineering
University of Auckland, Private Bag 92019, Auckland, New Zealand

[2] Institute for Energy Systems, School of Engineering, The University of Edinburgh, UK

Abstract

Leading edge vortices can create high local pressures which in some situations may be advantageous but in others may cause damage. This paper looks at three wind engineering situations: windborne debris, roof suctions on a low-rise building and pressures near the luff of a downwind sail, where the behaviour of the leading edge vortex is significant. In some of these situations the strength of the vortex varies in a random and intermittent manner while in others the process is directly linked to the motion of the structure.

Introduction

The importance of Leading Edge Vortices (LEV) is well known in low- Reynolds number aerodynamics as related to the flight of insects and small birds. For example Ellington et al. (1996) comment "Insects cannot fly, according to the conventional laws of aerodynamics: during flapping flight, their wings produce more lift than during steady motion at the same velocities and angles of attack." This foundational paper explains this enhanced lift in the following terms: "An intense leading-edge vortex was found on the downstroke, of sufficient strength to explain the high-lift forces." Martinez-Vazquez et al. (2012) show that in a similar manner the periodic formation of a strong LEV is important in the relatively high-Reynolds number behaviour of tumbling plates as encountered with windborne debris during extreme wind events. This situation will be discussed further in the following section.

There are a number of other high-Reynolds number situations where due to the geometry of the structure the flow separates from the leading of edge and, at least on average, reattaches at some point across the surface. In some situations, such as the conical vortices formed on delta wings, the LEV can be steady, but in many other situations the formation of an LEV may be intermittent. For example Li et al. (1999) discuss the statistics of peak pressures experienced under a leading edge vortex for a range of two-dimensional geometries and consider the significance of these for the action of fluctuating wind pressure on building cladding. In particular they note that the distribution is highly skewed towards high suction events. In this paper it is suggested that these high suction events are associated with the intermittent formation of a strong LEV which cannot be sustained indefinitely and is hence periodically shed into the flow.

A third high-Reynolds number application which appears to exhibit a combination of the characteristics of the tumbling plate and the intermittent LEV formation on a bluff body has been observed in the pressures near the leading edge of a downwind sail. In this case the motion of the yacht appears to stimulate the formation of a strong LEV which is then shed in a systematic manner. This phenomenon will be discussed in the final major section of this paper.

Windborne debris

In order to compute the trajectories of square plates a number of authors have suggested using lift and drag coefficients which are primarily based on static measurements. For example Holmes et al. (2006) show the static normal force coefficients measured in various wind tunnels and give the following fitted function

$$\begin{aligned} C_N &= 1.7(\alpha/40) \quad \text{for } \alpha<40^\circ \\ C_N &= 1.15 \quad \text{for } 40^\circ \le \alpha < 140^\circ \\ C_N &= 1.7(180-\alpha)/40 \quad \text{for } 140^\circ \le \alpha \le 180^\circ \end{aligned} \tag{1}$$

The normal force was resolved into drag and lift components, but an additional drag coefficient of 0.1 was been added to allow for the skin friction component. Thus

$$\begin{aligned} C_D &= 0.1 + C_N \sin(\alpha) \\ C_L &= C_N \cos(\alpha) \end{aligned} \tag{2}$$

However it was recognised that such static based forces do not tell the full story. Since Equation (1) is symmetric about α=90°, integration of Equation (2) over a 180° rotation results in a net drag force but no net lift. Tachikawa (1983) demonstrated that during autorotation of a square plate a net lift force did exist and hence Holmes et al. (2006) included a Magnus effect lift force to account for this.

The drag was determined from Equations (1-2) which give a mean drag coefficient of 0.83 and a maximum of 1.25. However both of these are significantly smaller than those measured by Tachikawa (1983) who gives mean drag coefficients of 1.19 and 1.21, for two slightly different thicknesses of square plate, and 1.29 and 1.31 for two thicknesses of aspect ratio two plates. He also shows that the typical maximum to minimum range was 3.0. These results show that under unsteady conditions, created by the rotation of the plate, the normal force coefficient can be much higher than obtained at any angle under static conditions.

It could be suggested that such high drag coefficients are unrealistic. However a simple experiment with a 1.5 g business card measuring 55 mm × 89 mm when launched from a height of 2.4 m, with a flick to initiate rotation, shows that it can travel forwards 1.8m while descending in a time of 1.8 s. The card very quickly locks into an autorotating decent at almost constant linear and angular speed and glide slope with the card rotating about its major axis of symmetry which is almost horizontal. Simple calculations show that the card's mean speed is 1.67 m/s, the glide angle is 53° and hence the mean drag and lift coefficients are 1.42 and 1.06 respectively. Since the drag coefficient will be very small when the card is parallel to the flow it is clear that the maximum drag coefficient must be around 2.8.

In recent years researchers from the Universities of Birmingham, Nottingham and Auckland have carried out both experimental and CFD analyses of a rotating square plates (Martinez-Vazquez et al. 2011 & 2012). The experimental programme used square plates up to 1m × 1m, with embedded differential pressure transducers. The largest plate contained 24 pressure transducers connected to six data loggers. It was mounted on a horizontal shaft and was observed to autorotate with a tip speed ratio around 0.3. Figure 1 shows an example of the normal force coefficient variation with angle of attack where the maximum value is 2.75, which occurred when the plate was almost normal to the flow and hence the maximum drag coefficient is of similar magnitude. One of the important features of these results is the fact that they do not show any sign of the stall seen in all static measurements at an angle of attack of 40°. Instead the normal force continues to increase well beyond that which occurs at any static angle. The average drag force coefficient, calculated using Equation (2), is 1.15, 38% higher than estimated from static force measurements. These high mean drag coefficients are important for windborne debris since it is primarily the drag force that determines how quickly the object will accelerate towards the wind speed, which indirectly affects the objects damage potential.

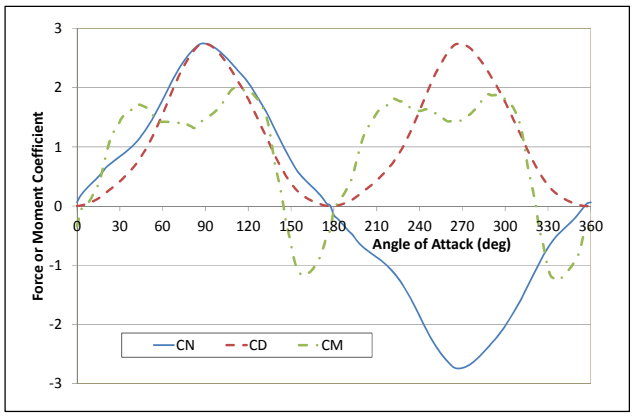

Figure 1. Normal force, drag force and pitching moment coefficients as a function of angle of attack determined by pressure integration. Wind speed 10 m/s.

Martinez-Vazquez et al. (2012), in discussing the CFD results, explain the flow behaviour in the following terms: “The flow is characterized by a pronounced leading-edge vortex that forms and remains attached to the plate’s retreating edge (upper edge) and is eventually shed into the wake. This attached vortex, which has been observed to create artificial lift during insect flight (Wang 2005) and in the auto-rotation of Maple seeds (Lentink et al. 2009), is attributed to the low pressure vortex core close to the plate that amplifies the differential pressures at the retreating edge of the plate. The advancing edge (lower edge) of the plate has shown weaker vortices that form due to stretching and roll-up of the vortex sheet at the trailing edge, and are quickly shed.” It appears that at low angles of attack the flow over the upper surface separates at the leading edge but is able to reattach. The vorticity generated at the leading edge is hence fed into the LEV which strengthens and is held near the surface by the retreating plate until sometime after α=90°. In contrast the flow separating from the lower surface at the trailing edge has no chance to reattach and so the vorticity is shed into the shear layer which forms an arc along the lower edge of the wake. A shaft mounted plate will autorotate in either direction depending on the initial angle of attack, whereas the above descriptions assume that the leading edge is moving upwards since free falling plates will always lock onto this direction of rotation. Once a plate has started to rotate in one direction this is sustained since the strong LEV always forms on the leeward side of the retreating edge, which provides a moment to maintain that rotation. As illustrated in Figure 1 the moment coefficient can be positive for most of the cycle, which is necessary to overcome the bearing friction. If the plate was to rotate very slowly the quasi-static moments would cancel out, however with moderate rotation the formation and shedding of the LEV provides a moment which initially accelerates the angular velocity. As the tip speed ratio (TSR) increases several factors will tend to weaken the LEV including:

- As the angular velocity increases the relative velocity of the flow around the leading edge weakens which will decrease the rate of generation of vorticity.
- The time available to form the LEV will reduce which will tend to reduce the strength of the LEV.
- The increased angular velocity will modify the angle of the flow near the leading edge which may alter the formation or shedding of the LEV.

All of these weaken the driving moments until it is balanced by opposing moment, mostly due to the positive pressures on the windward side of the advancing half, and a steady rotation is achieved. Both Tachikawa (1983) and Martinez-Vazquez (2012) observed that the asymptotic tip speed ratio was of the order of 0.3 for a square plate. Tachikawa (1983) reports a slightly higher limiting TSR of 0.45-0.48 for aspect ratio two plates, while the free flying aspect ratio four cardboard plate reported by Richards et al. (2005) had a TSR=0.59. It appears that the limiting TSR increases with aspect ratio although the latter result may also reflect absence of bearing resistance with free flying plates.

From this analysis the following observations may be made:

1. Given the right conditions an LEV can be created which results in differential pressures that are stronger than would occur in a static situation.
2. The average force created in a transient situation may be stronger than the steady value.
3. The associated moments tend to drive autorotation although these appear to weaken as the TSR increases.

Low-rise building wind loading

Leading edge vortex dynamics can also be important for static structures such as low rise buildings. Richards and Hoxey (2011 a&b) note that under certain conditions the minimum pressures measured on the Silsoe 6m Cube were significantly lower than might be expected from quasi-steady analysis. This particularly affected taps on the windward half of the sidewalls and roof when the wind was almost perpendicular to one face. During some experiments sonic anemometers were placed alongside (0.5 m from the centreline) Taps V8 – V11 (see Figure 2). These measured the velocity components approximately 60 mm from the roof surface. Figure 3 shows the probability density functions for the streamwise component of velocity (U) from the reference and four roof sonic anemometers.

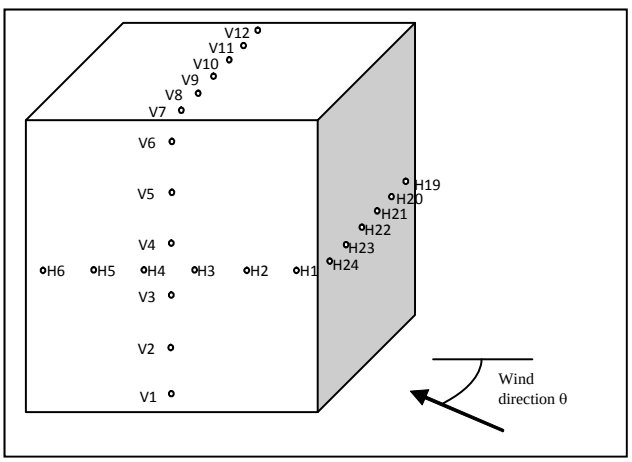

Figure 2. Tap locations on the Silsoe Cube

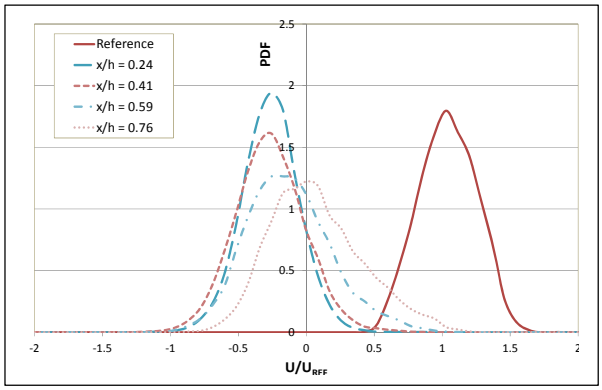

Figure 3. Probability density functions for the U velocity component at the reference anemometer and for four sonic anemometers lying alongside Taps V8-V11. The mean wind direction was 86.5°, almost perpendicular to the windward face.

The velocity data shows that most of the time the windward half of the roof experiences reversed flow which suggests the existence of an LEV-type flow. In contrast the point three-quarters of the way across the roof (x/h = 0.76) only experiences reverse flow for 40% of the time. Flow visualisation (see Richards and Hoxey 2011 b) shows that the LEV is very unsteady, at times extending across most of the roof while at other times it tightens and is then shed into the flow, before being re-established.

Observation of time histories for the taps on the roof, see Figure 4(a), shows that the minimum pressure peaks appear to be short duration spikes, primarily affecting taps V7-9. The form of these spikes can be clarified by expanding the area around the most negative of these spikes (Figure 4(b)). This reveals a sequence of events which affects all of the taps on the roof.

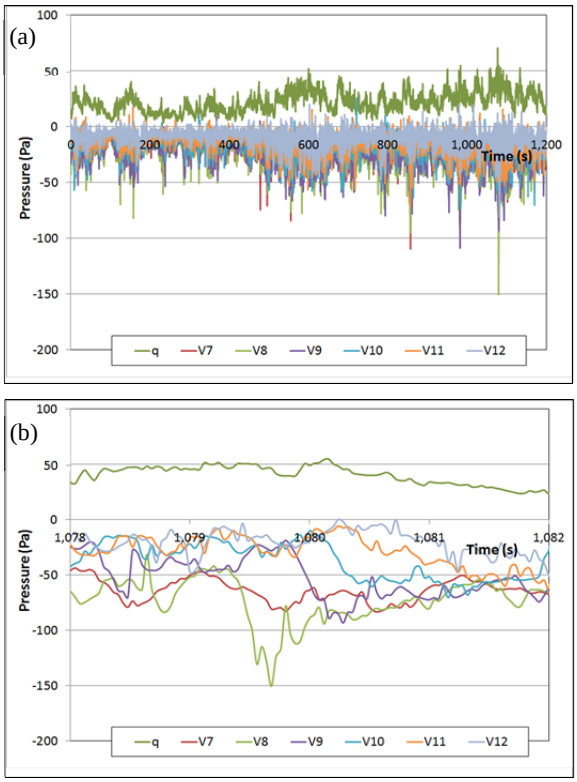

Figure 4. Full-scale pressure data from one 20 minute run during which the wind direction was θ=86.5°; (a) time histories for the reference dynamic pressure q and the roof pressures, and (b) the same pressures expanded around the time of the lowest pressure which occurred at Tap V8 at a time of 1079.7s.

This particular event occurs when the reference dynamic pressure is well above the 20 minute average of 22 Pa, but does not appear to be associated with a strong gust of duration similar to the spike. The pattern of these events is made clearer by conditionally averaging close to these peaks. The trigger used here is when the pressure at Tap V8 is a local minimum and exceeds a threshold pressure equal to the mean pressure coefficient for that tap times the maximum dynamic pressure recorded in that record. The results are shown in Figure 5(a), where the pattern has been averaged over 19 events. The time has been normalised such that unit time represents the time needed for the reference wind occurring around the time of the event to move one cube height. The pattern observed does appear to be a characteristic of this flow since a similar pattern has been observed in Large Eddy Simulations of this flow (see Richards and Norris 2014) and in wind tunnel modelling at the University of Auckland as shown in Figure 5(b). The conditionally averaged U velocities from the four roof sonic anemometers are shown in Figure 5(c). It is noticeable that at the time the pressure at Tap V8 nears its minimum there is a strong reversed flow nearby. This tends to confirm that these spikes are caused by the temporary formation of a tight vortex over the windward half of the roof, which is then shed and travels across the roof.

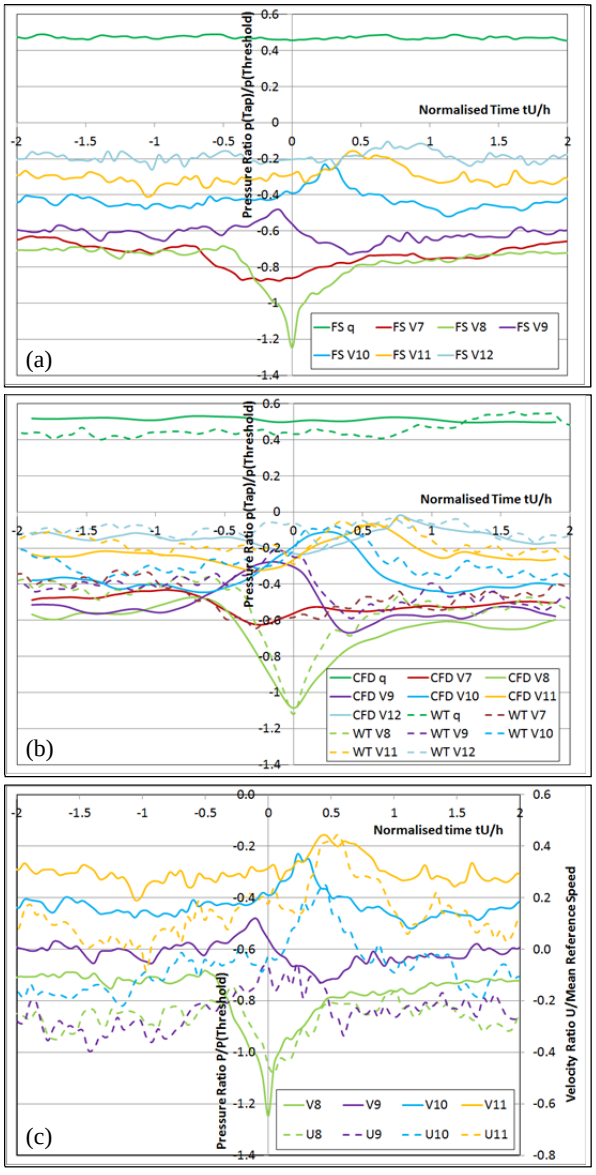

Figure 5. Conditionally averaged result around pressure spikes: (a) From full-scale, (b) From CFD and wind tunnel and (c) full-scale pressures for Taps V8-11 along with the nearby velocities.

Downwind sail pressures

A similar sequence of pressure pulses has been observed on downwind sails. The University of Auckland Yacht Research Unit has measured the differential pressures on an asymmetric spinnaker and mainsail (for details of the system see Motta et al 2014). The transducers were arranged in five horizontal stripe on the spinnaker and three stripes on the mainsail. Figure 6 shows the pressures measured on the spinnaker over a 30s period. It can be seen that the highest differential pressures (lightest colours) occur on the 4/5th stripe near the top of the spinnaker and always occur near the luff (leading edge, which is the bottom edge of the band). A high differential pressure event seems to develop at approximately 1.7s intervals. These pressure fluctuations are highly correlated with the pitching motion of the yacht, what is not clear is whether this correlation is a matter of "cause" or "effect". Once the pressure near the luff reaches its peak the pulse then seems to spread across the sail.

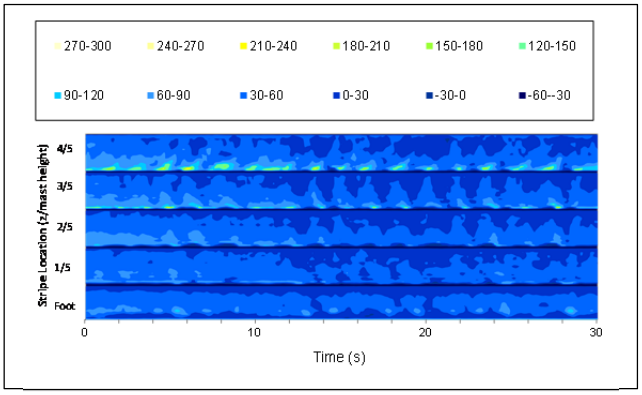

Figure 6. Spatio-temporal evolution of the differential pressures on an asymmetric spinnaker. The horizontal axis is time while the vertical axis is split into five bands, one for each stripe. Within each band the vertical position is the fractional distance across the local chord, with the luff (leading edge) at the bottom.

In order to highlight the sequence of events occurring at the 4/5th stripe Figure 7 shows the conditionally averaged pressures. The trigger used was the peak pressure at the second transducer. It can be seen that the peak pressure coefficient is over seven times the highest dynamic pressure recorded by the masthead anemometer around the time of the event. This is about double than which might be expected from wind tunnel or CFD studies such as Viola et al. (2014).

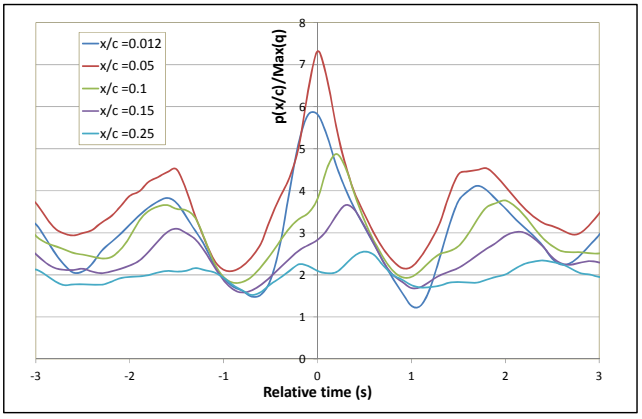

Figure 7. Conditionally averaged differential pressures on the 4/5th stripe. The trigger event used was the peak pressure at the second tap in the stripe (x/c=0.05). The pressures were normalised using the maximum dynamic pressure recorded by the masthead anemometer within ±2s of the event.

The sequence of pressure pulses suggests the formation and shedding of an LEV. With both this situation and the cube roof pressures it appears that as the vortex is shed it lifts away from the surface and hence the surface pressures become weaker.

Conclusions

Leading edge vortices can often give rise to high suction pressures and hence may lead to high forces. In some situations, such as a tumbling plate, the formation and behaviour of the LEV is driven by the movement of the structure. In other situations, such as on the roof of low-rise buildings, the LEV appears to randomly vary in strength, with the occasional formation of a strong vortex along with the associated high suction pressures. However such a strong LEV is not sustainable and so it is shed into the flow. Finally the LEV on the upper section of an asymmetric spinnaker shows some links with each of these situations, the formation of a strong LEV is stimulated by the yachts motion, but once formed this is shed into the flow.

References

Ellington CP, Van den Berg C, Willmot AP, Thomas ALR (1996) Leading-edge vortices in insect flight, Nature (London) 384, 626-630

Lentink D, Dickson WB, van Leeuwen JL, Dickinson MH (2009) Leading-edge vortices elevate lift of autorotating plant seeds, Science, 324(5933), 1438-1440.

Li QS, Calderone I, Melbourne WH (1999) Probabilistic characteristics of pressure fluctuations in separated and reattaching flows for various free-stream turbulence, J. Wind Eng. Ind. Aerodyn. 82, 125-145

Martinez-Vazquez P, Sterling M, Baker CJ, Quinn A, Richards PJ, (2011) Autorotation of square plates, with application to windborne debris, Journal of Wind and Structures 14(2), 167-186.

Martinez-Vazquez P, Kakimba B, Sterling M, Baker CJ, Quinn AD, Richards PJ, Owen JS (2012) Pressure field of a rotating square plate with application to windborne debris, Journal of Wind and Structures 15 (6), 527-547

Motta D, Flay RGJ, Richards PJ, Le Pelley DJ, Deparday J, Bot P (2014) Experimental investigation of asymmetric spinnaker aerodynamics using pressure and sail shape measurements, Ocean Engineering, 90, 104-118

Richards PJ, Hoxey RP, (2011a & b) Pressures on a cubic building-Part 1: Full-scale results & Part 2: Quasi-steady and other processes. J. Wind Eng. Ind. Aerodyn., 102, 72-86 & 87-96.

Richards PJ, Norris SE, (2014) LES modelling of unsteady flow around the Silsoe cube, Computational Wind Engineering 2014 Conference, Hamburg, Germany, 8-12 June 2014.

Richards PJ, Williams N, Laing B, (2005) 3-Dimensional aerodynamics and motion of plate type wind-borne debris'. 6th Asia-Pacific Conference on Wind Engineering, Seoul, Korea, 12-14 September, 762-777.

Tachikawa M, (1983) Trajectories of flat plates in uniform flow with application to wind-generated missiles, J. Wind Eng. Ind. Aerodyn., 14, 443-453.

Viola IM, Bartesaghi S, Van-Renterghem T, Ponzini R, (2014) Detached Eddy Simulation of a sailing yacht, Ocean Eng. 90, 93-103.

Wang ZJ, (2005) Dissecting insect flight, Annu. Rev. Fluid Mech., 37, 183-21